Electronic Supplementary Material (ESI) for ChemComm.

Optimized Full CO_2 Photoreduction Process by Defective Spinel Atomic Layers

Yang Wu[2,+], Dongpo He[1,+], Lei Li[2,+], Zhiqiang Wang[2], Wensheng Yan[2], Junfa Zhu[2], Yang Pan[2], Qingxia Chen[1,*], Xingchen Jiao[1,*], Yi Xie[2]

[1]Key Laboratory of Synthetic and Biological Colloids, Ministry of Education, School of Chemical and Material Engineering, Jiangnan University, Wuxi 214122, China.
[+]These authors contributed equally to this work.
[2]Hefei National Research Center for Physical Sciences at Microscale, National Synchrotron Radiation Laboratory, University of Science and Technology of China, Hefei 230026, China.
*Corresponding author.
Email: qxchen@jiangnan.edu.cn; xcjiao@jiangnan.edu.cn

EXPERIMENTAL SECTION

Synthesis of the $ZnGa_2O_4$ atomic layers:

220 mg $Zn(CH_3COO)_2 \cdot 2H_2O$ dissolved in 20 mL of deionized water, then 512 mg $Ga(NO_3)_3$ was added by stirring for 20 min, followed by 10 mL of anhydrous ethylenediamine. After 10 min of magnetic stirring, the liquid was transferred to a 50 mL Teflon lined hydrothermal autoclave, heated at 180 °C for 24 h, and then removed and cooled naturally at room temperature. The obtained white precipitate was washed with water and ethanol for several times, and then dried vacuum overnight to obtain $ZnGa_2O_4$ atomic layers.

Synthesis of the defective $ZnGa_2O_4$ atomic layers:

The obtained white $ZnGa_2O_4$ nanosheets were heated at 600 °C in a 5% H_2/Ar atmosphere for 1 h, and then removed and cooled naturally at room temperature. The collected solid powder was used for progressive characterization and denoted as defective $ZnGa_2O_4$ atomic layers.

Characterization:

TEM images were performed with a JEOL-2010 TEM with an acceleration voltage of 200 kV. HRTEM images were carried out on a JEOL JEM-ARM200F TEM/STEM with a spherical aberration corrector. XRD patterns were obtained from a Philips X'Pert Pro Super diffractometer with Cu Kα radiation (λ = 1.54178 Å). UV−vis diffuse reflectance spectra were measured on a Perkin Elmer Lambda 950 UV−vis−NIR spectrophotometer. XPS spectra were acquired on an ESCALAB MKII system with Al Kα (*hv* = 1486.6 eV) as the excitation source. The binding energies obtained in the XPS spectral analysis were corrected for specimen charging by referencing C 1s to 284.8 eV. *In situ* FTIR spectra were obtained by using a Thermo Scientific Nicolet iS50. Synchrotron-radiation photoemission spectroscopy (SRPES), X-ray absorption near-edge spectroscopy (XANES) spectra, and SVUV-PIMS spectra were executed at the National Synchrotron Radiation Laboratory (NSRL) in Hefei, China. BET surface area was acquired on automatic microporous gas adsorption analyzer system (ASAP 2020 M PLUS).

Photocatalytic CO_2 reduction measurements:

The photocatalytic CO_2 reduction measurements were conducted in a sealed off-line reactor (Perfect light Limited, Beijing). In the CO_2 photocatalytic conversion process, 5 mg $ZnGa_2O_4$ powders were initially dispersed in 1 mL deionized water and then spined dropped onto a quartz glass. After heating at 60 °C for 30 minutes, the $ZnGa_2O_4$ powders were successfully deposited on the quartz glass (diameter: 3.6 cm and area: 10.2 cm^2). After putting the quartz glass in the reaction cell as well as injecting 10 mL deionized water on the bottom, the reaction cell was vacuum-treated for three times, which was then pumped by high-purity CO_2 (99.99%) to reach an atmospheric pressure. The light irradiation comes from a CEL-HXF300 Xe lamp (Beijing China Education Au-light Co., Ltd.) with a standard AM 1.5G filter and cut 400 nm filter, outputting the light density of about 100 mW/cm^2, calibrated by an CEL-NP2000 Optical Power Meter (Beijing China Education Au-light Co., Ltd.). The instrument was initially pumped and purged for three times, which was then filled by 99.99% high-purity CO_2 to reach an atmospheric pressure. During the

light irradiation, the evolved gas products were qualitatively examined by Agilent GC-7890B gas chromatograph equipped with flame ionization detector (FID) and thermal conductivity detector (TCD) while ultrahigh-purity argon was used as a carrier gas.

Apparent quantum yield (AQY) experiments:

The apparent quantum yield (AQY) was calculated as the ratio between the number of photogenerated electrons consumption and the number of incident photons, by taking into account the fact that two electrons are required to produce one CH_3COOH molecule. The wavelength-dependent AQY was measured under the same photocatalytic reaction condition, except for the monochromatic light wavelengths (450, 550, and 650 nm).

***In situ* FTIR spectra experiments:**

In situ FTIR spectra were obtained by using a Thermo Scientific Nicolet iS50, equipped with an MCT detector cooled by liquid nitrogen and a commercial reaction chamber from Harrick Scientific. After degassed at 100 ℃ in N_2 atmosphere for 20 min, the gas flow was switched to high-purity CO_2 (99.99%) for adsorption. The background spectrum was collected after 30 minutes of adsorption in high-purity CO_2. Each spectrum was recorded by averaging 64 scans at a 4 cm^{-1} spectral resolution.

DFT calculation details:

The first-principles calculations were performed with the Vienna ab initio simulation package.[1] The interaction between ions and valence electrons was described using projector augmented wave (PAW) potentials, and the exchange-correlation between electrons was treated through using the generalized gradient approximation (GGA) in the Perdew-Burke-Ernzerhof (PBE) form.[2] To achieve the accurate density of the electronic states, the plane wave cutoff energy was 480 eV. The ionic relaxations for all structures in the calculations were carried out under the conventional energy (10^{-3} eV) and force (0.01 eV/Å) convergence criteria. The $ZnGa_2O_4$ slab along the [001] projection was used to mimic the as-prepared nanosheets, where a 1.5 nm vacuum layer was added to avoid interactions.

Gibbs free energies for each gaseous and adsorbed species were calculated at 298.15 K, according to the expression:

$$G = E_{DFT} + E_{ZPE} - TS$$

$$E_{ZPE} = \sum_i 1/2\ h\nu_i$$

$$\Theta_i = h\nu_i / k$$

$$S = \sum_i R[\ln (1-e^{-\Theta i/T})^{-1} + \Theta_i/T\ (e^{\Theta i/T} - 1)^{-1}]$$

where E_{DFT} is the electronic energy calculated for specified geometrical structures, E_{ZPE} is the zero-point energy, S is the entropy, h is the Planck constant, ν is the computed vibrational frequencies, Θ is the characteristic temperature of vibration, k is the Boltzmann constant, and R is the molar gas constant. For adsorbates, all 3N degrees of freedom were treated as frustrated harmonic vibrations with negligible contributions from the catalysts' surfaces. In the computational hydrogen electrode (CHE) model,[3] each reaction step was treated as a simultaneous transfer of the proton-electron pair as a function of the applied potential. Thus, free energy changes can be represented by

$$\Delta G[COOH^*] = G[COOH^*] + G[H^+ + e^-] - (G[^*] + G[CO_2] + 2\times G[H^+ + e^-])$$

$$\Delta G[CO^*] = G[CO^*] + G[H_2O] - (G[^*] + G[CO_2] + 2\times G[H^+ + e^-])$$

$$G\ [H^+ + e^-] = 1/2\ G\ [H_2] - e\ U$$

where U is the applied overpotential and e is the elementary charge.

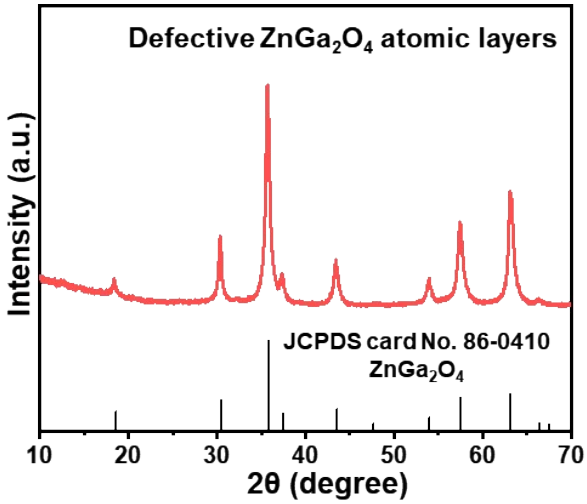

Figure S1. XRD pattern for the defective $ZnGa_2O_4$ atomic layers.

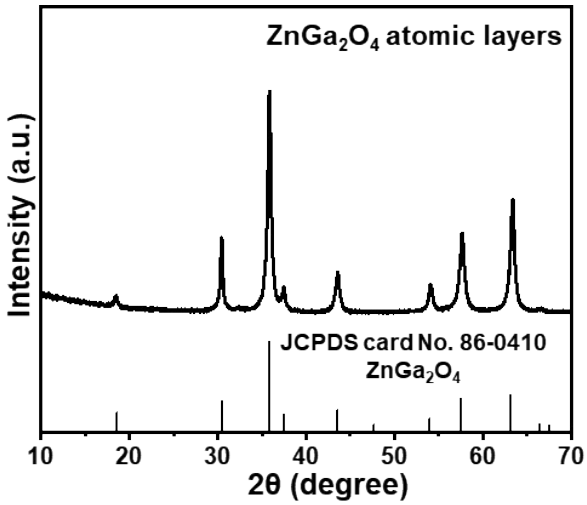

Figure S2. XRD pattern for the $ZnGa_2O_4$ atomic layers.

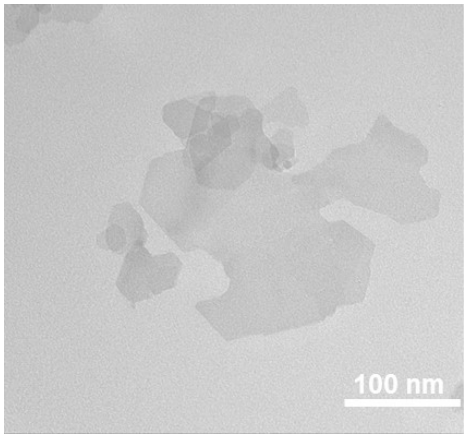

Figure S3. TEM image for the $ZnGa_2O_4$ atomic layers.

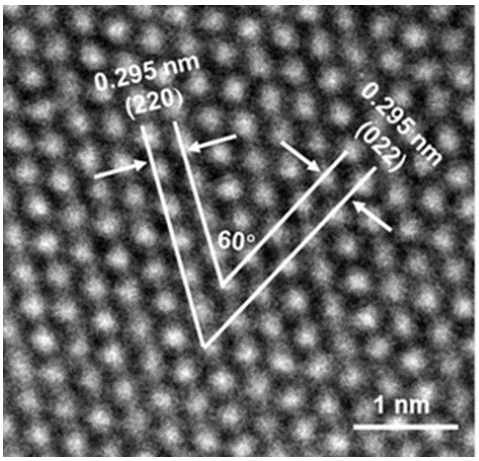

Figure S4. HRTEM image for the $ZnGa_2O_4$ atomic layers.

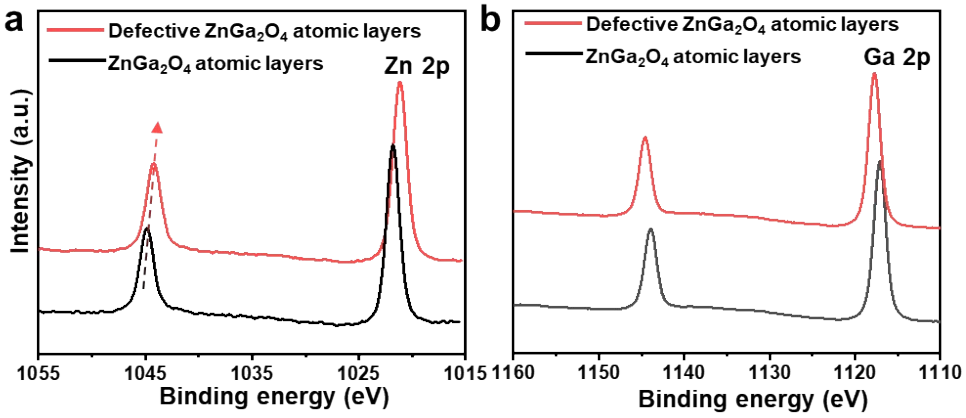

Figure S5. (a) Zn 2p and (b) Ga 2p XPS spectra a for the defective $ZnGa_2O_4$ atomic layers and the $ZnGa_2O_4$ atomic layers.

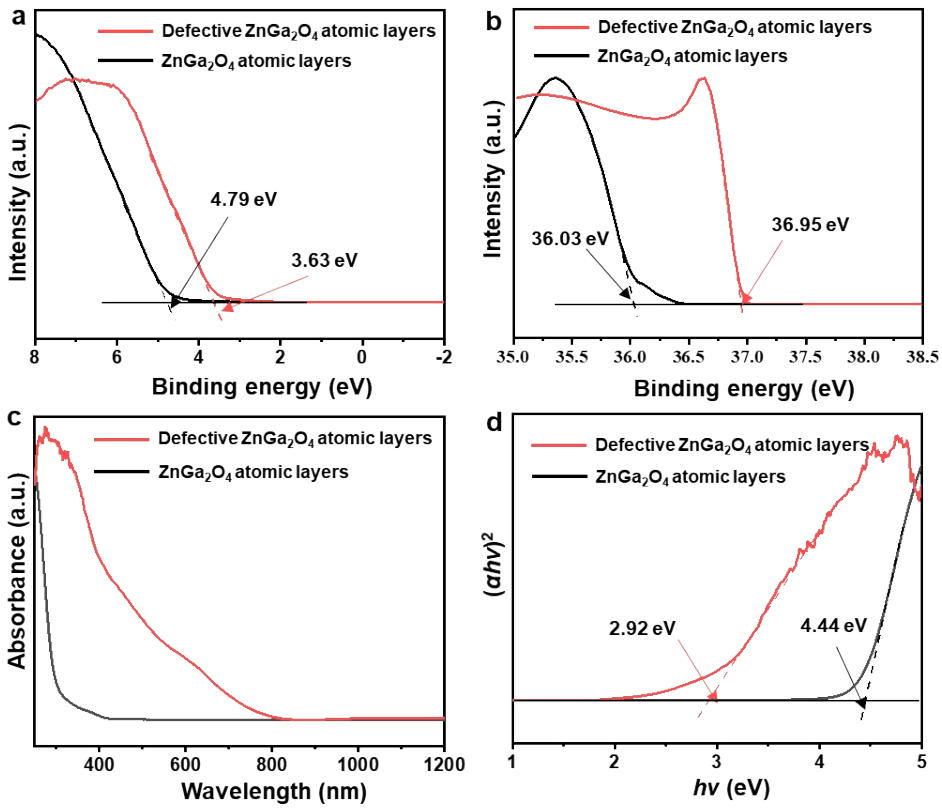

Figure S6. Experimental results concerning the electronic band structures. (a) Valence-band position, (b) the secondary electron cutoff energy measured by synchrotron-radiation SRPES spectra, (c) UV−vis diffuse reflectance spectra and (d) the band gaps based on UV-vis diffuse reflectance spectra for the defective $ZnGa_2O_4$ atomic layers and the $ZnGa_2O_4$ atomic layers.

Figure S6a indicated the work functions for the $ZnGa_2O_4$ atomic layers and the defective $ZnGa_2O_4$ atomic layers could be calculated to be 4.79 and 3.63 V, respectively. Meanwhile, Figure S6b showed their valence band (VB) maximum were 3.97 and 3.05 V vs. vacuum level, respectively. Hence, the defective $ZnGa_2O_4$ atomic layers and the $ZnGa_2O_4$ atomic layers possessed the VB maximum of 1.77 and 3.85 V vs. normal hydrogen electrode (NHE) at pH 7, respectively. The UV-vis diffuse reflectance spectra (UV-DRS) displayed that the defective $ZnGa_2O_4$ atomic layers and the $ZnGa_2O_4$ atomic layers had the optical bandgaps of 2.92 and 4.44 V, respectively (Figure S6c-d). Based on synchrotron-radiation photoemission spectroscopy (SRPES) and UV-DRS spectra, the conduction band (CB) minimum for the defective $ZnGa_2O_4$

atomic layers and the $ZnGa_2O_4$ atomic layers located at ca. -1.15 and −0.59 V vs. NHE at pH 7.

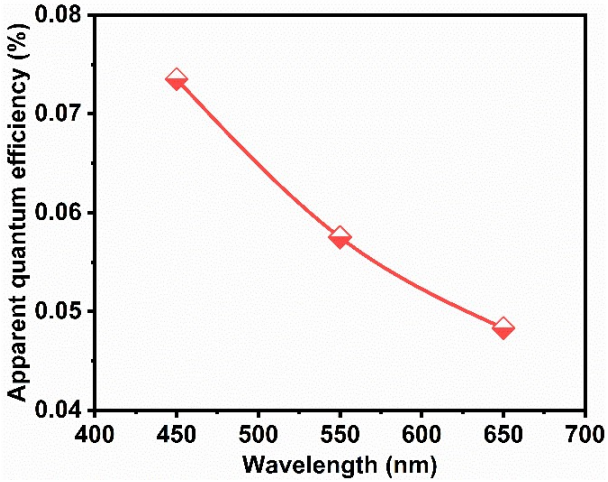

Figure S7. AQY values of CO_2 photoreduction to CO over the defective $ZnGa_2O_4$ atomic layers.

Figure S7 showed the measured AQY of CO evolution for the defective $ZnGa_2O_4$ atomic layers, in which the AQY under the wavelength of 450 nm was about 0.074%.

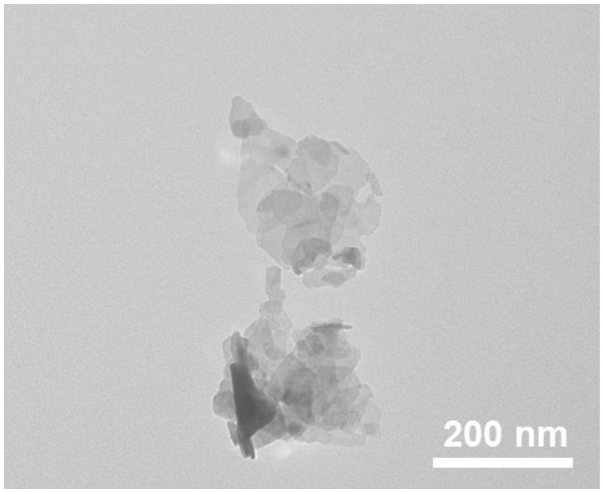

Figure S8. TEM image for the defective $ZnGa_2O_4$ atomic layers after photocatalysis.

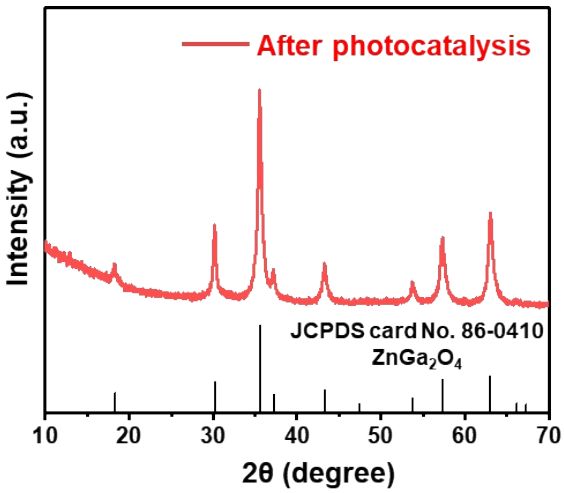

Figure S9. XRD patterns for the defective $ZnGa_2O_4$ atomic layers after photocatalysis.

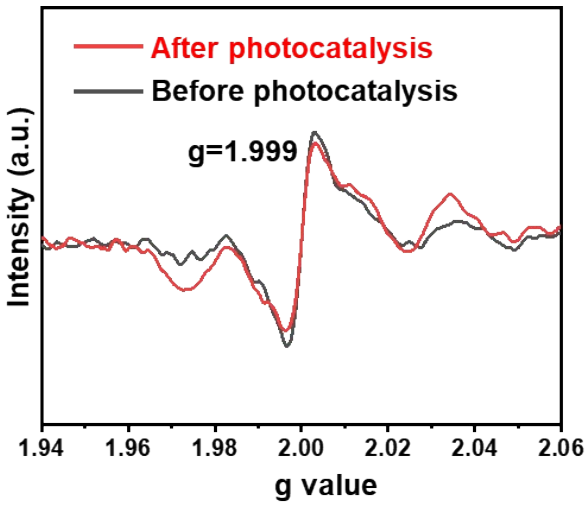

Figure S10. EPR spectra for the defective $ZnGa_2O_4$ atomic layers before and after photocatalysis, in which the pattern of "Before catalysis" was indexed to that of the defective $ZnGa_2O_4$ atomic layers in Figure 1d.

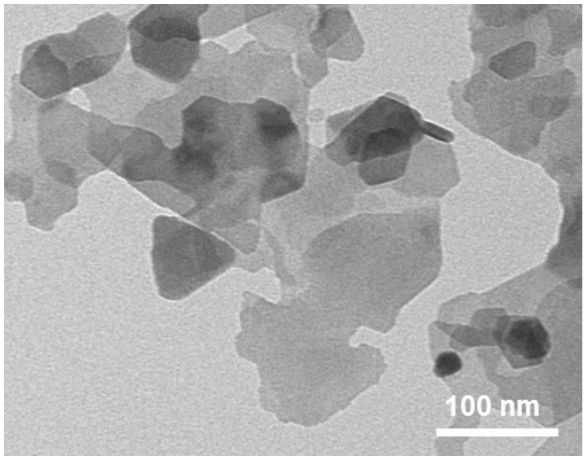

Figure S11. TEM image for the $ZnGa_2O_4$ atomic layers after photocatalysis.

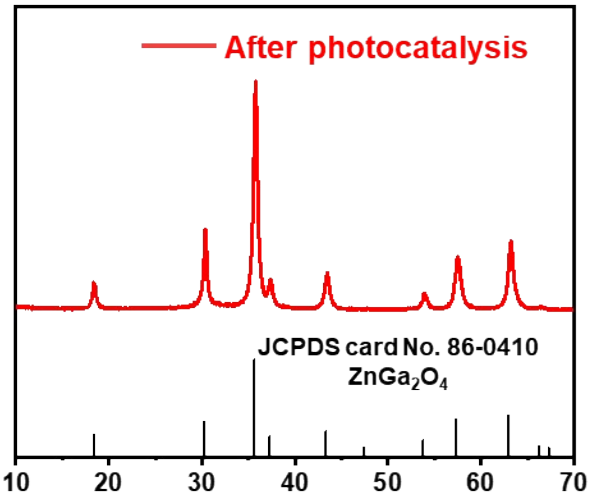

Figure S12. XRD patterns for the $ZnGa_2O_4$ atomic layers after photocatalysis.

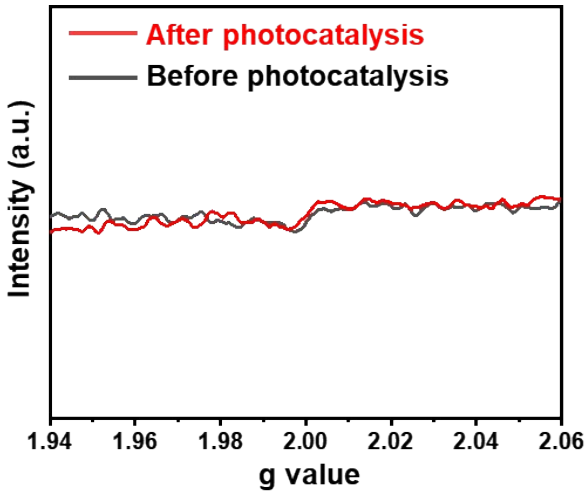

Figure S13. EPR spectra for the $ZnGa_2O_4$ atomic layers before and after photocatalysis,

in which the pattern of "Before catalysis" was indexed to that of the $ZnGa_2O_4$ atomic layers in Figure 1d.

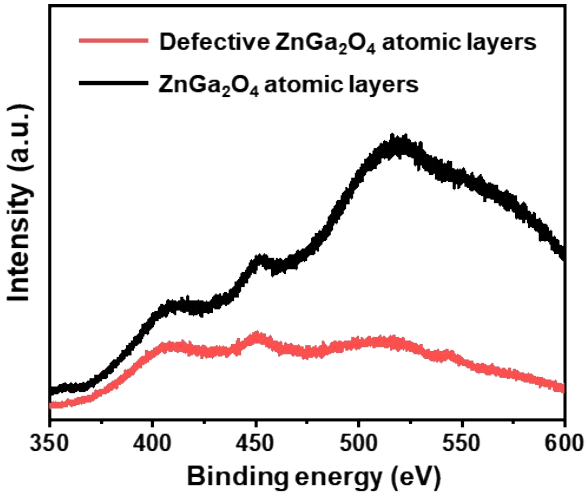

Figure S14. PL spectra for the defective $ZnGa_2O_4$ atomic layers and the $ZnGa_2O_4$ atomic layers.

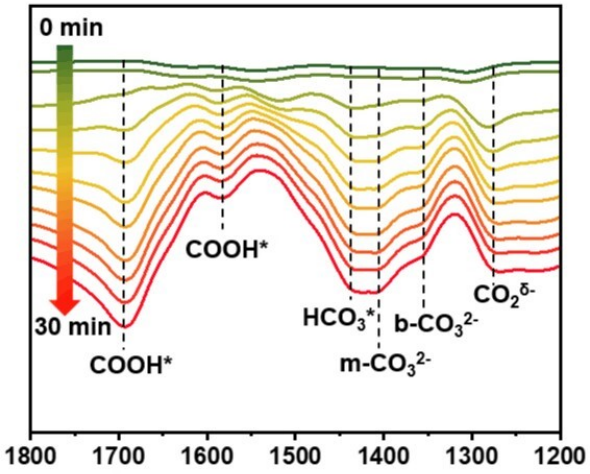

Figure S15. *In situ* FTIR spectra for the $ZnGa_2O_4$ atomic layers during CO_2 photoreduction.

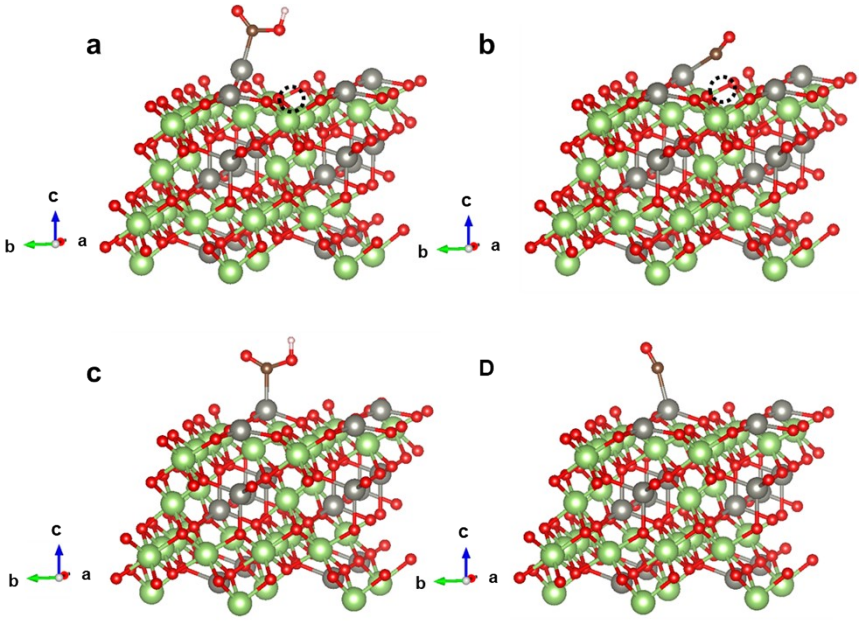

Figure S16. Schematic diagrams for the configurations of the key COOH* intermediate of (a) the defective $ZnGa_2O_4$ atomic layers and (c) the $ZnGa_2O_4$ atomic layers. Schematic diagrams for the configurations of the key CO* intermediate of (b) the defective $ZnGa_2O_4$ atomic layers and (d) the $ZnGa_2O_4$ atomic layers. The gray, green, and red globules represent Zn, Ga, and O atoms, respectively, and the black dotted circle corresponds to the location of the oxygen vacancy.

Table S1: Free energy (eV) correction for the species during CO_2 photoreduction over the defective $ZnGa_2O_4$ atomic layers and the $ZnGa_2O_4$ atomic layers slabs.

Species	E_{DFT}	ZPE	TΔS
H_2O	-14.21	0.56	0.67
CO_2	-22.98	0.31	0.66
H_2	-6.76	0.27	0.40
CO	-14.79	0.13	0.6
CO_2^*		0.35	0.13
$COOH^*$	/	0.66	0.16
CO*	/	0.24	0.11

Table S2: The DFT-calculated energy without correction (eV) of the defective $ZnGa_2O_4$ atomic layer slab and the $ZnGa_2O_4$ atomic layer slab as well as the corresponding intermediates during CO_2 photoreduction.

Samples	E_{DEF} (*)	E_{DFT} (CO_2*)	E_{DFT} (COOH*)	E_{DFT} (CO*)
defective $ZnGa_2O_4$ atomic layer slab	-606.69	-629.93	-632.04	-622.25
$ZnGa_2O_4$ atomic layer slab	-611.53	-634.76	-636.50	-626.79

Table S3: Free energy (eV) of CO_2 photoreduction for the defective $ZnGa_2O_4$ atomic layer slab and the $ZnGa_2O_4$ atomic layer slab.

Samples	△G (*+CO_2)	△G (CO_2*)	△G (COOH*)	△G (CO*)	△G (*+CO)
defective $ZnGa_2O_4$ atomic layer slab	0	0.30	1.93	0.59	0.69
$ZnGa_2O_4$ atomic layer slab	0	0.31	2.30	0.88	0.69

References

[1] G. F. Kresse, *J. Comput. Mater. Sci* **1996**, *6*, 15−50.

[2] Y. K. Y. Zhang, W. T., *Phys. Rev. Lett.* **1998**, *80*, 890−890.

[3] B. H. Hammer, L. B.; Nørskov., *J. K. Phys. Rev. B* **1999**, *59*, 7413–7421.